Journal of Natural Disaster Science, Volume 26, Number 1, 2004, pp15-26

Instrumented Model Slope Failure due to Water Seepage

Rolando P. ORENSE[1], Suguru SHIMOMA[2],
Kengo MAEDA[3] and Ikuo TOWHATA[3]

[1]Chuo Kaihatsu Corporation, Shinjuku-ku, Tokyo, Japan
[2]Shimizu Corporation, Tohoku Branch, Iwate, Japan
[3]Department of Civil Engineering, University of Tokyo, Japan

(Received for 20. Oct., 2003 and in revised from 15 Sep., 2004)

ABSTRACT

Many slope failures have been observed to occur during or immediately after rainfall. Although conditions leading to these failures have been described as caused by a rapid rise in pore-water pressure as a result of rainwater infiltration, the important factors that influence the initiation of slope failures have not been adequately clarified. To investigate these factors, a series of laboratory experiments was conducted on model sandy slopes to determine the initiation process of rainfall-induced slope failure. In the tests, failures were induced in small-scale model slopes either by water percolation from the side upslope or by artificial rain falling on top of the slope. Besides monitoring pore-water pressure, changes in soil moisture contents and ground deformation were measured. Test results showed that slope failure was always induced when the soil moisture content within a certain region near the toe of the slope reached nearly full saturation, even though other parts of the sliding mass were still in a partially saturated state. In addition, minute deformations along the slope were shown to precede failure. The findings presented here show that by monitoring the soil moisture content of slopes and performing displacement measurements, it is possible to predict the occurrence of rainfall-induced slope failure.

1. INTRODUCTION

Landslides induced by heavy rainfall often occur on marginally stable slopes that consist of various types of soil, such as colluvial and residual ones. Because of its frequency and proximity of various infrastructure developments to landslide-prone areas, rainfall-induced slope instability is considered one of the most significant geo-environmental hazards.

Mitigation of damage caused by rainfall-induced slope failures can be classified broadly in two categories; hard-type approaches, such as slope stabilization methods as in the use of retaining walls, dewatering techniques, anchor piles, etc. and soft-type approaches, such as implementing appropriate alarm and warning systems. Considering the extent of potentially unstable slopes, the first category may not always be feasible due to financial and environmental constraints. Monitoring systems therefore offer viable alternatives. In some locations, e.g., Hong Kong (Brand et al., 1984), the San Francisco Bay area (Keefer et al., 1987), Honolulu (Wilson et al., 1992), and Japan (Okada and Sugiyama, 2001), warning systems have been established to help minimize risk. In general, they are based on correlations between rainfall intensity and the landslide frequency and are highly empirical because current understanding of the mechanisms and conditions leading to rain-induced failure is not sufficient to develop an efficient warning system.

To establish accurate warning systems, efforts have focused on understanding the mechanism and conditions leading to these failures and on formulating procedures to predict their occurrence. Monitoring of various indices, such as deformation (Sasahara, 2001), pore-water pressure (Yagi and Yatabe, 1987), soil suction (Kitamura et al., 1999), groundwater depth (Yokota et al., 2000) and acoustic emissions (Kousteni et al., 1999), at critical locations within a slope is being considered as a basis for prediction. In experimental study presented here, not only pore-water pressure, but soil moisture content and ground deformation were measured by innovative types of sensors. The findings can be used to formulate site-specific warning systems to minimize damage caused by slope failures.

2. EXAMPLES OF LANDSLIDES CAUSED BY RAINFALL

Thousands of landslides occurred on the Boso Peninsula, Chiba Prefecture (Japan) due to rainfall during the passage of Typhoon No. 25 which struck the eastern part of the Japanese mainland in September 1971. The peninsula is about 140 km long and 50 km wide. Its mountains, such as the Boso Hills, generally are not high (in the 200-300 m range). Fig. 1 shows the distribution of slope failures on the peninsula. More than 1,000 were reported in Shibayama Town (dark zone in the figure), which has an area of approximately 1 km^2. Another town which was hit severely was Omigawa in the northeastern part of the peninsula, where more than 250 landslides were reported. Based on the official description of the disaster caused by this event reported by

KEY WORDS: slope failure, rainfall, seepage, model test, soil moisture content

Chiba Prefecture (1972), precipitation in the Omigawa area from the evening of September 6 to the morning of September 7 was 106 mm, with a maximum hourly rainfall of 42 mm.

Some of the landslides in Omigawa have been investigated extensively by Fukuoka (1980) and Yoshida et al. (1991a, 1991b). Slopes in the area rise about 50 m above the alluvial plain near the mouth of the Tone River. Terrains predominantly consist of cemented silty sands, but near slope surfaces, the soil is fragmented by tree roots to a depth of about 2-3 m and exists in a loose to medium dense state. Slope failure took place at shallow depths in the disintegrated soil layer near the surface. Based on his findings, Fukuoka (1980) enumerated the causes of these landslides. One is a decrease in the shearing resistance of the soil resulting from an increase in soil moisture content. Another is an increase in unit weight due to the increase in soil moisture content. Other causes include surface erosion and an increase in pore water pressure in faults or joints.

Based on the above causes, the increase in soil moisture content associated with rainwater infiltration is significant in inducing slope failure. Fukouka (1980) stressed that to analyze the stability of slopes during rainfall, it is necessary to know the change in the saturation ratio and the strength parameters of highly saturated soils.

With this in mind, a series of laboratory model tests were performed on small-scale model slopes using sandy materials obtained from a landslide site in Omigawa. The objectives were to investigate the process of rainfall-induced slope failures and to clarify the parameters essential for failure initiation. The tests focused on detailed observations of the failure process and temporal development of soil moisture contents during water infiltration. It should be noted that the tests were not intended to simulate the failure of real slopes, in which non-uniformities that are related to soil conditions, topographical features, boundary conditions, and rainfall patterns normally exist.

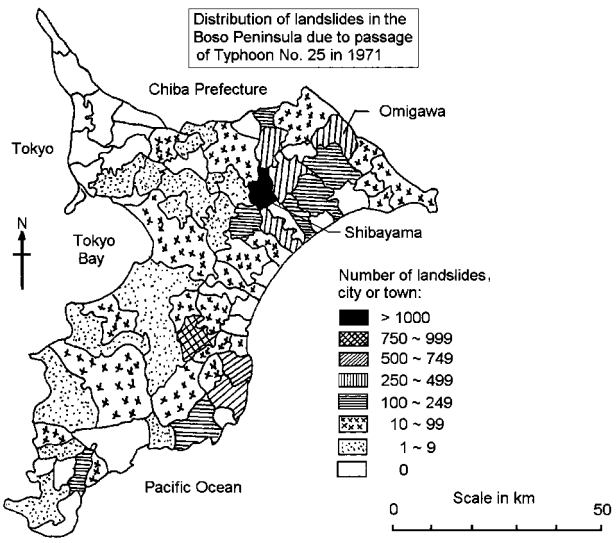

Fig. 1 Location map of Omigawa and the distributions of number of slope failures in the Boso Peninsula, Chiba Prefecture caused by Typhoon No. 25 in 1971 (after Fukuoka, 1980)

3. EXPERIMENTAL OUTLINE

3.1 Materials Used

The soil samples used were obtained from a landslide site in Omigawa (discussed in Section 2). The material is silty sand, with a Fc=9% fines content and the fines are non-plastic. Physical properties and grain size distribution curve are given in Fig. 2. The shear strength parameters in the figure correspond to those of a sample with Dr=60% relative density obtained in conventional drained triaxial compression tests. In addition, the soil water characteristic curves of Omigawa sand obtained from water retentivity tests are shown in Fig. 3. Note that for this soil, the air entry value (defined as the magnitude of matric suction that must be exceeded before air recedes into the soil pores) is about 2 kPa, which is considered typical for granular materials.

3.2 Experimental Box and Transducers

The tank used in the model tests is shown schematically in Fig. 4. It is 220cm long, 80cm wide and 100cm high. Its walls are made of steel plates, except for the front one which is made of acryl glass for easy observation of the deformation process. The box is divided into three sections; a central portion 197cm long that is used to construct the slope and left and right chambers, each 11.5cm wide, respectively used to supply and drain the water. Perforated steel walls covered with wire mesh divide these three sections to allow the easy movement of water through them without washing out the soil grains. The left outer wall of the box adjacent to the water supply chamber has small rectangular openings with covers that are positioned at appropriate locations (see Fig. 5).

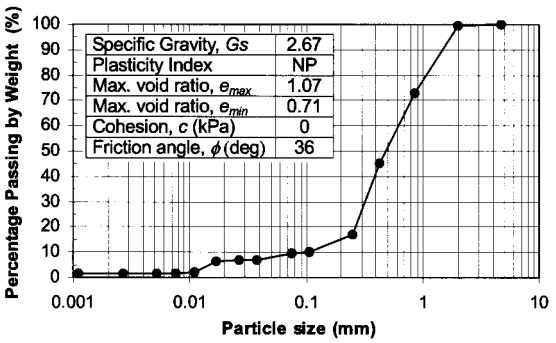

Fig. 2 Grain size distribution curve and physical properties of the soil used

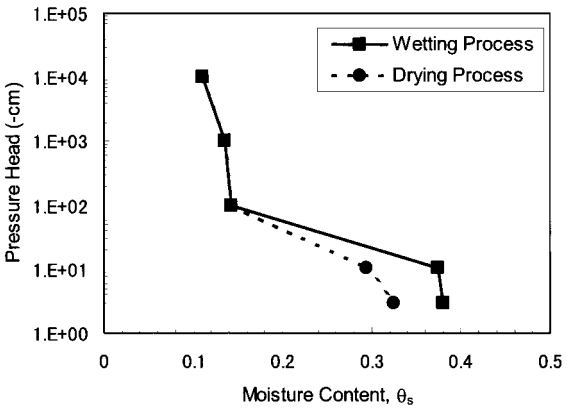

Fig. 3 Soil water characteristic curves for Omigawa soil

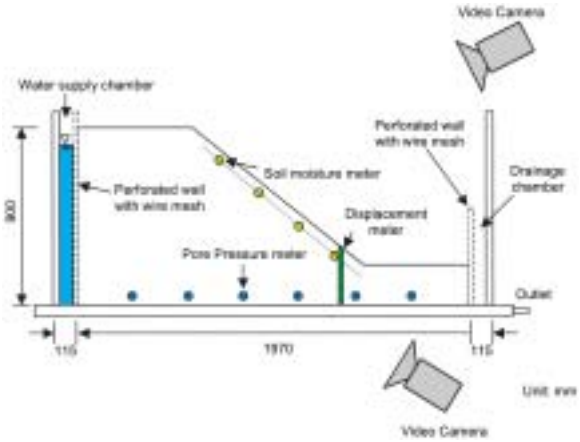

Fig. 4 Schematic diagram of the experimental slope model and the sensor locations

Fig. 5 Photo of the experimental soil box

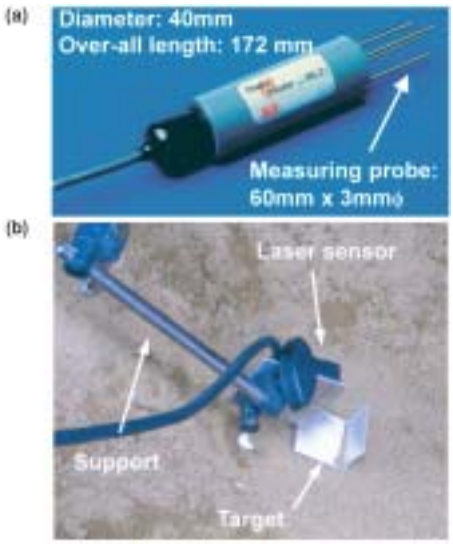

Fig. 6 Photos of: (a) an ADR-type soil moisture sensor; (b) a laser displacement sensor

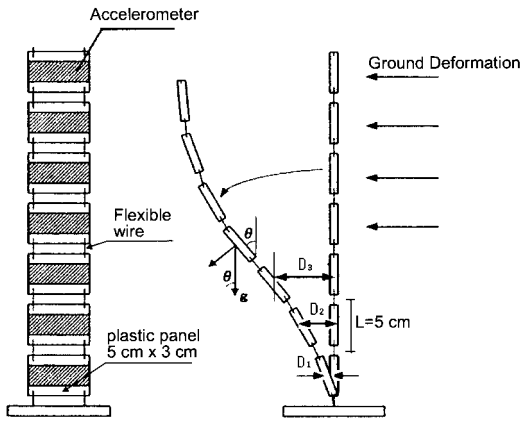

Fig. 7 Structure of shear displacement transducer. Left: plan view; Right: lateral view showing a deformed configuration

These openings can be uncovered to allow water to flow out of the supply chamber if there is need to maintain a desired water elevation within the chamber; i.e., to keep a constant head at the ingress point.

Various sensors, such as pore-water pressure meters, soil moisture content transducers, and shear displacement transducer, were installed in the model slope, as shown schematically in Fig. 4. All the sensors were connected to a computer-based data acquisition system.

Two sets of pore-water pressure meters were used in the tests: one with a capacity of 20 kPa, the other 100 kPa. The soil moisture sensor used, shown in Fig. 6(a), is the ADR (Amplitude Domain Reflectometry) type. It measures the change in impedance between the probe body of the sensor and the ground in which the sensing head (array of four rods) is embedded. The relative impedance gives the dielectric constant of the ground, a measure of the volumetric water content, θs, the ratio of the volume of water in the soil pores to the total volume. Note that the dielectric constant of water (80) is significantly greater than that of the other soil matrix materials (3-4) and of air (1); therefore, the dielectric constant of the soil primarily depends on the soil moisture content. This type of sensor gives a stable reading within 1-5 sec, and can measure volumetric moisture content to within ±5% (based on generalized calibrations) or even ±1% (with soil-specific calibrations). It can read data in soils even with high salinity levels and is not affected by temperature (Muñoz-Carpena, 2004). Because of its standard circuitry, it is relatively inexpensive and provides the same level of accuracy and ease of use as the more popular but costly TDR (time domain reflectometry) and capacitance insertion probes (Wijaya et al., 2002). In our tests, prior to installation the sensor was appropriately calibrated on Omigawa sand to obtain the correlation between the moisture content and the sensor output.

A shear displacement transducer was installed near the toe of the slope to monitor variations in sub-surface deformation with time. This transducer is similar to that originally developed by Sasaki et al. (1991) and consists of 3cm high by 5cm wide plastic panels with an accelerometer attached to each panel. These are connected vertically by flexible wire (Fig. 7). Considering the in-between spacing, each panel has an effective height of 5cm. The bottom part of the panel assembly is fixed to the base of the box.

During ground displacement, the panel system is displaced and, based on the acceleration recorded at each panel, the degree of tilt of each one can be estimated. Starting from the lowermost panel, the lateral displacement of each one is calculated, from which values the lateral displacement of the whole panel system, assumed to be equivalent to the lateral deformation of the ground, can be assessed. With this transducer, the residual (or static) component of the recorded acceleration in each panel can be separated from the dynamic (or vibrating) component by performing Fourier analysis, after which it is expressed in terms of the acceleration due to gravity in order to calculate the degree of tilt of the panel. This is shown schematically on the right in Fig. 7.

In some tests, surface displacement also was measured by placing targets securely on the slope surface and monitoring their movement with a laser displacement transducer fixed in support adjacent to the target (see Fig. 6b). This sensor uses a high precision laser beam which can detect infinitesimal displacements within 10μm, thereby providing extremely accurate measurements of minute displacements of the slope surface. The readings are fairly straight-forward, showing a linear relationship between the analog output and detected distance. Moreover, it detects objects with very low surface reflection characteristics, such as black rubber. Because the beam is easy to aim, precise positioning and alignment are possible.

In addition to the displacement transducers, pin markers were placed on the slope surface and on the side of the model ground adjacent to the acryl glass wall (Fig. 5). In some tests, horizontal lines consisting of kaolin clay also were laid out on the surface of the slope and served as reference lines during the deformation process. Two video cameras were set-up at strategic points, respectively to monitor displacement of the side and the surface of the model slope.

3.3 Experimental Program

In the experiments, homogenous model soil slopes were constructed in the central portion of the box by laying out Omigawa soil with the initial (gravimetric) water content of w=10% in series of horizontal layers. Each layer was tamped equally with a tamping rod to obtain the prescribed height. This procedure was repeated until the full height of the model slope was obtained. The various sensors described earlier were installed in the slope at specified locations as soil placement progressed.

In the experiments, effects of the initial relative density, Dr, slope inclination, α, slope configuration and seepage operation were examined. Two types of models, shown in Fig. 8, were considered. Model A consisted of homogenous sloping ground that was 90cm thick upslope and 20cm thick downslope, giving a net model slope height equal to 70cm. Model B consisted of homogenous sloping ground with constant thickness, h. The impermeable soil base was constructed by dumping soil into the box and covering its surface with a vinyl sheet which then was fastened to the interior walls to prevent water infiltration into the soil base. Sandpaper was glued to the upper portion of the sheet to prevent any sliding of soil on top of the layer. The model slope subsequently was constructed over this impermeable base.

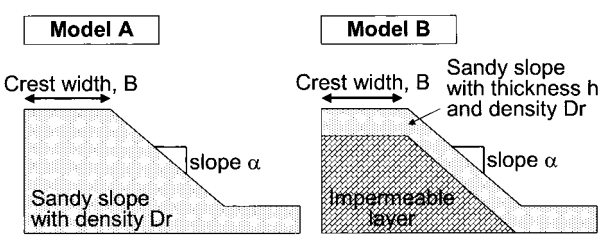

Fig. 8 Two types of model slopes used in the experiment

After preparing the model slope, failure was initiated by seepage from the top of the slope (hereafter seepage tests) or by artificial rainfall (hereafter rainfall tests). In the seepage tests, infiltration was simulated by introducing water into the upslope section of the model slope through the water supply chamber (Fig. 4). The water level in this chamber was increased to the specified elevation of 80cm and maintained at that level throughout the experiment by spilling out the excess water through the small windows built into the outer wall of the experimental box. This process effectively replicated the effects of groundwater flow from upper locations on natural slopes. In the rainfall tests, instability was induced by infiltrating water through hoses and nozzles set-up adjacent to the experimental box (Fig. 9). To minimize water infiltration between the impermeable sidewalls of the box and the adjacent soil, water-resistant plastic strips were used to seal the boundaries. Efforts were made to keep the rainfall intensity, r, constant, both in time and space. Varying the rainfall pattern as occurs in actual situations was not attempted. Therefore such patterns are beyond the scope of this study. Rainfall gauges were placed at two locations, one at the top, another at the bottom of the slope. The accumulated rainwater was measured periodically to determine the rainfall intensity.

The experimental program is outlined in Table 1. Slope inclination was changed from α=30-40 degrees, and the relative densi-

Fig. 9 Experimental set-up for the artificial rainfall test

Table 1. Experimental program

Case No.	Type of test	Model Type	Remarks
1	Seepage	A	α=40°, B=60 cm, Dr=50% (Reference case)
2	Seepage	A	α=30°, B=38.5 cm, Dr=50%
3	Seepage	A	Same as Case 1 except Dr=70%
4	Rainfall	A	Same as Case 1 with r=70-96 mm/h
5	Rainfall	A	Same as Case 1 with r=154 mm/h
6	Seepage	A	Same as Case 1 (to confirm reproducibility)
7	Seepage	A	Same as Case 1 except B=30 cm
8	Rainfall	B	Same as Case 1 with h=20 cm, r=80-262 mm/h
9	Rainfall	B	Same as Case 1 with h=30 cm, r=42-72 mm/h

ty from Dr=50-70%. These values were deemed to represent typical conditions in natural soil slopes. Tests were terminated (both water infiltration and data recording were stopped) when sufficient slope failure had been observed. It should be noted that the number of transducers installed in the model slope varied depending on sensor availability at the time the tests were conducted.

Experimental results for Cases 1-3 have been reported by Orense et al. (2002), and those for Cases 4-5 by Shimoma et al. (2002). Only the experimental results for the remaining four cases therefore are discussed in detail here. For completeness of presentation, a summary of the major findings for Cases 1-5, however, is included.

4. EXPERIMENTAL RESULTS

4.1 Seepage Tests

4.1.1 Case 6

The slope in Case 6 is the Model A type with an initial relative density of Dr=50%, slope inclination of α=40°, and crest width of B=60cm. The water level at the supply chamber was maintained at the height of 80cm, and, with the difference in the pressure head within the model ground, water was allowed to percolate through the soil. About 48 minutes after the start of water infiltration, slope failure started to occur due to the formation of tension cracks near the lower part of the slope adjacent to the steel wall. Thereafter this failure propagated to other parts of the slope. In general, the failure surfaces formed were the non-circular retrogressive type. Slope movement within the model ground terminated several minutes after the onset of failure.

Fig. 10 shows the time histories of monitored sub-surface deformation near the toe of the slope, volumetric moisture content, θs, and pore water pressure (P.W.P.) at the sensor locations (also depicted in the figure). Soil moisture sensors were installed at d=5cm from the surface of the slope. The progress of the wetting front within the model ground is clear in Fig. 10(c), in which the increase in pore-water pressure recorded starting from P4 to P1 indicates gradual formation of the water table from left to right, analogous to the direction of seepage flow.

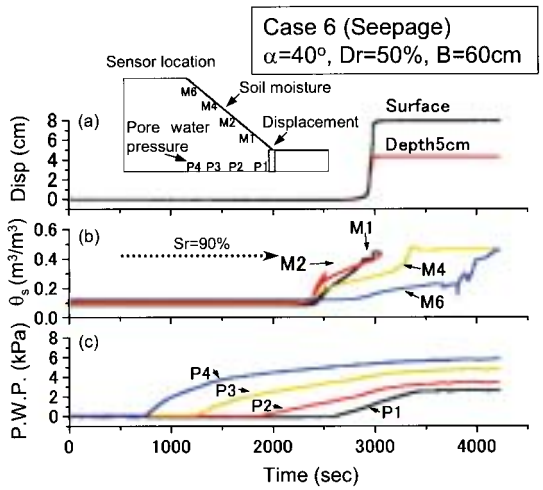

Fig. 10 Time histories of: (a) toe displacement; (b) volumetric water content, θs; (c) pore-water pressure (P.W.P.) for Case 6

About 2400 sec after the test began, the wetting front reached the locations of the soil moisture sensors, and a rapid increase in moisture content was recorded near the toe of the slope (M1 and M2). After some time had passed, minute slope movement occurred, as evidenced by the displacement time history in Fig. 10(a). When the volumetric water content in this region reached θs=0.42, equivalent to the degree of saturation Sr=90%, large deformation was triggered near the toe. This deformation was extremely rapid, reaching a maximum surface displacement of 8cm within a few seconds (Fig. 10(a)). In contrast, maximum deformation of 4cm was monitored 5cm below the surface, indicative that only the surficial portion of the downslope was involved in the sliding process. These findings are consistent with those obtained with the video cameras which showed that in the upslope section, a portion about 15-20cm thick slid down the slope (Fig. 11). It should be stated that during the deformation process, soil moisture sensors M1 and M2 were displaced by the moving ground, causing erratic readings. Sensor readings therefore were terminated at that time (see Fig. 10(b)).

As indicated in Table 1, Case 6 was designed to reproduce the results of Case 1, presented elsewhere (Orense 2002). In Case 1, pore-water pressure meters were not available and generated pore pressures were calculated by FEM-based seepage analysis. The comparison of the results for Cases 1 and 6 shows that the failure initiation phenomena, as well as the progress of failure, were very similar. Fig. 11 shows the inclination of the slope before and after failure in Case 6. It is notable that in all the tests performed, the average slope angle after failure was about 20°. Subsequent calculations showed that this is the minimum inclination (i.e., factor of safety, F_s=1.0) of an infinite slope with the friction angle ϕ=36°(the same as that of Omigawa sand) under seepage flow.

4.1.2 Case 7

In Case 6, saturation in the lower half of the slope surface initiated the slope failure. To examine what happens when most of the slope surface becomes saturated, Case 7, which had a similar slope but a narrower crest width (B=30cm), was investigated. With this type of model ground, the phreatic surface induced by percolating water was considered to develop parallel to the slope. Moreover, to monitor minute deformation of the slope, a target was fixed on its surface near the toe, and a laser displacement transducer was used to record displacement of the target along the

Fig. 11 Photo showing the model slope after the test (Case 6)

direction of the slope.

In Case 7, the start of mass movement was registered about 23 minutes after the start of water infiltration. Collapse began near the bottom half of the slope adjacent to the steel wall and propagated upward to the other parts of the slope. Compared with the failure in Case 6, the video images taken by the cameras showed more rapid progression of movement and failure involving almost the entire slope occurred in less than a minute. This was because the entire slope was in almost fully saturated state and therefore had lower strength. As in Case 6, non-circular retrogressive failure surfaces were present.

The time histories recorded by the sensors as well as the sensor locations are shown in Fig. 12. As in Case 6, the advance of the wetting front is evident from the time history of the pore-water pressure (Fig. 12(d)), but unlike that case, the wetting front reached the topmost soil moisture sensor (M4) first, and saturation started near the top of slope and moved toward the bottom (Fig. 12(c)). Initially, the rise in the volumetric water content was rapid then became gradual as the ground approached full saturation. When the volumetric water content at M1 reached θs=0.42 (about Sr=90%), deformation with maximum surface displacement of about 3cm was triggered at the toe. Again, only the surficial portion of the slope was involved in the flow. Movement of the target placed near the toe of slope, obtained by the laser displacement sensor shown in Fig. 12(b), was consistent with that obtained by the shear displacement transducer. A more detailed discussion of the deformation measurements obtained by the laser sensor is presented in a later section.

It is interesting that deformation of the ground did not start even when the upper (M4) and middle (M3, M2) portions of the slope were almost saturated (Sr>90%). In fact, deformation of the slope began only when there was almost full-saturation near the toe of the slope. This means that saturation at any point within a slope will not result in slope failure; rather, movement is initiated only when the most critical region, in this case the toe of the slope, becomes saturated. Nevertheless, the high degree of saturation over the whole slope contributed to the rapid propagation of failure. Fig. 13 shows the deformed configuration of the slope after the test. Although movement affected almost the entire slope, failure generally involved only the superficial portion of the slope.

The moisture content distribution after slope failure was verified by obtaining soil samples from various locations at the end of the test. Moisture contents were determined in the laboratory by the conventional procedure. Although not presented here, the values obtained by sampling clearly agreed with those obtained by the moisture sensors at the end of the test.

4.1.3 Saturated Zone Distributions

To understand the role of the saturated zone in slope deformation, pore-water pressure heads within the slope (monitored by pore pressure meters installed at the bottom of the box) were calculated and plotted. Distributions of the saturated zone for the slopes in Cases 6 and 7 at the time of slope failure are shown in Fig. 14.

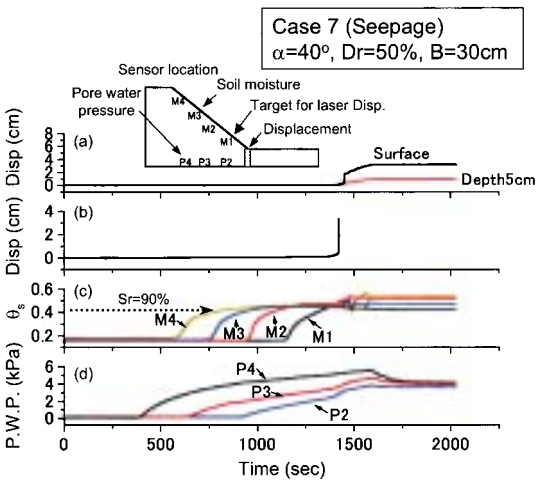

Fig. 12 Time histories of: (a) toe displacement by the shear displacement transducer; (b) target displacement by the laser displacement sensor; (c) volumetric water content, θs; (d) pore-water pressure (P.W.P.) for Case 7

Fig. 13 Photo showing the model slope after the test (Case 7)

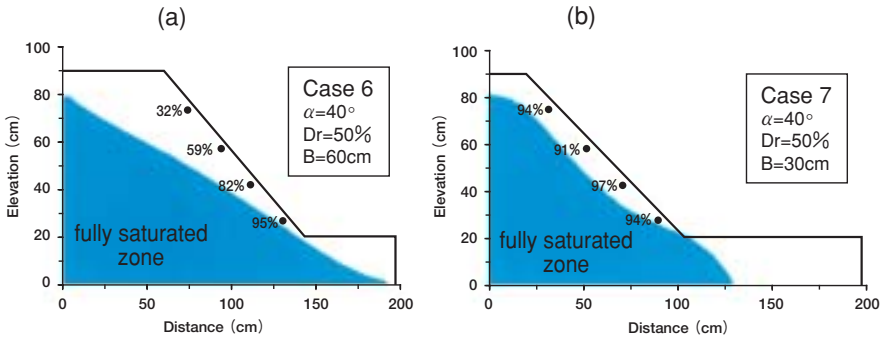

Fig. 14 Distributions of saturated zone at the time of failure: (a) Case 6; (b) Case 7 (seepage tests)

The shaded portions correspond to fully saturated regions within the model ground whose upper boundaries correspond to piezometric levels. Numbers adjacent to the slope (expressed in percent) represent the *Sr* as monitored by the soil moisture sensors (shown by black dots) located 5cm below the slope surface. For Case 7, the water table is almost parallel to the slope, inducing a high moisture content over the entire slope. In comparison, the upper portion of the slope in Case 6 is far from the phreatic surface; therefore lower soil moisture contents were recorded at this location.

4.2 Rainfall Tests

4.2.1 Case 8

A slope with the Model B type of configuration was used in Case 8. The thickness of the deposit was set at h=20cm. Artificial rain was sprinkled on top of the slope through a hose positioned outside the box, with its nozzle directed over the entire exposed slope surface. The actual rainfall intensity, r, was obtained by monitoring the rainwater that accumulated at rainfall gauges positioned at the top and at the bottom of the slope. Fig. 15 shows variation in cumulative rainfall over time at these two locations. The plots of the data points have almost constant slopes during the duration of the experiment, evidence of constant intensity at each location. The upslope registered greater intensity (r=262 mm/h) than the downslope (r=80 mm/h), however, because it was nearer the source of rainfall.

Fig. 16 gives the time histories of ground displacement, soil moisture contents, and pore-water pressures monitored from the onset of rainfall. Fig. 16(b) shows that when infiltrating rainwater reached the sensor locations (at t=800-900 sec), soil moisture contents at all locations increased simultaneously. Upon reaching values of about θs=0.22-0.25, they remained constant as the wetting front progressed downward toward the impermeable base. Upon reaching that base, water accumulated and a water table formed (t=2200 sec), specifically in the lower half of the slope, as shown by the increase in pore water pressure (P1, P2, P4) in Fig. 16(c). The water table continued to rise upward and on reaching the soil moisture sensor locations, the soil moisture content (at sensors M2, M3, M4) increased again. Note that the pore-water pressure at the P5 location near the top of the slope did not increase, possibly because rainwater did not accumulate there but flowed down the slope. Consequently, sensor M5 did not register much of an increase in soil moisture during the initial phase of the test.

At t=1800 sec, a crack began to appear near the top of the slope (Fig. 17(a)). At t=3500 sec, when the soil moisture sensor near the toe (M2) registered θs=0.43 (corresponding to Sr=91%), the slope slowly began to move but stopped 200 sec later. When the volumetric water content near the top (M5) began to increase however, probably as a result of water infiltrating through the crack formed adjacent to the sensor, the entire slope suddenly began to move as a whole. Unfortunately, this movement was not captured by the shear displacement sensor installed at the slope

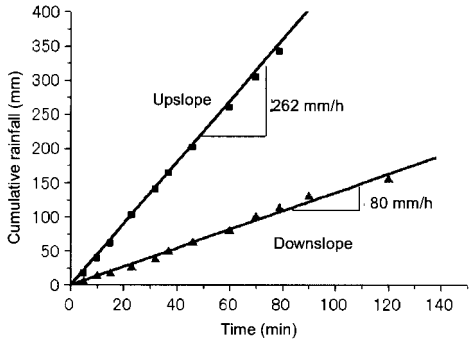

Fig. 15 Accumulated rainfall vs. time upslope and downslope in the model ground (Case 8)

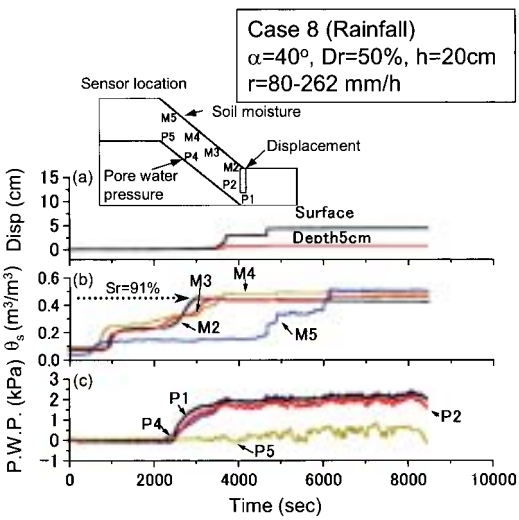

Fig. 16 Time histories of: (a) toe displacement; (b) volumetric water content, θs; (c) pore-water pressure (P.W.P.) for Case 8

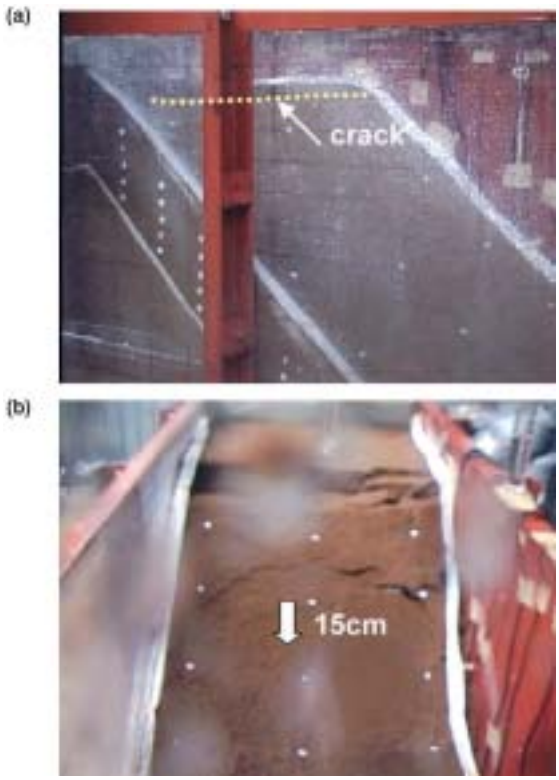

Fig. 17 (a) Formation of a crack near the top of the slope prior to failure; (b) Photo showing the upslope area undergoing 15 cm displacement

bottom. Video footage, shown in Fig. 17(b), confirmed that the entire slope underwent about 15cm movement.

4.2.2 Case 9

A similar model slope was used in Case 9, except that the thickness of the ground was set at h=30cm. In addition, the rainfall intensity was decreased to r=42-72 mm/h. Details of the recorded rainfall intensity are given in Fig. 18.

The recorded time histories are shown in Fig. 19. As in Case 8, the rise in volumetric water content was a two-step process.

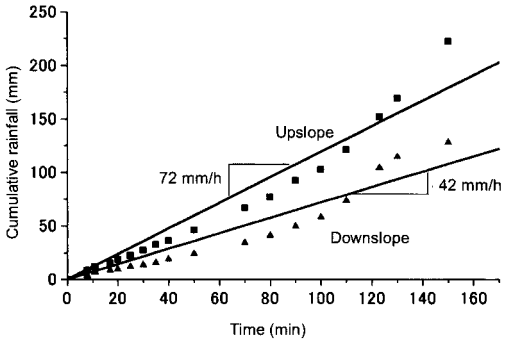

Fig. 18 Accumulated rainfall vs. time upslope and downslope in the model ground (Case 9)

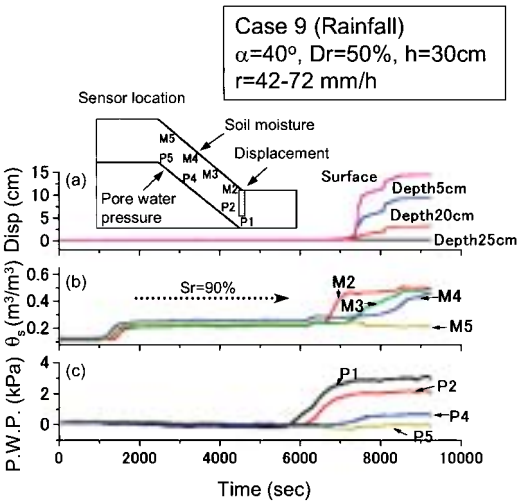

Fig. 19 Time histories of: (a) toe displacement; (b) volumetric water content, θs; (c) pore-water pressure (P.W.P.) for Case 9

After reaching a value of θs=0.22-0.25, all the soil moisture content readings remained constant, indicative that the rate of infiltration within the model ground was relatively constant. A water table began to develop near the toe of the slope at t=6000 sec, corresponding to the time the wetting front reached the base. Note that the time required to develop this water table was longer than in Case 8 because of the lower rainfall intensity and thicker depth through which rainwater needed to percolate to reach the base. The water table formed only near the bottom portion of the base (P1, P2). Rainwater at the top of the slope probably flowed downward, preventing an accumulation of water in the top portion. As the water table near the toe rose, the wetting front also moved upward, causing an increase in the volumetric water content near the surface soil at the slope toe (M2).

At about t=7000 sec, surface cracks perpendicular to the direction of the slope started to form near the top of the slope, and small-scale deformation occurred but soon stopped. When the region at the toe became saturated (θs=0.42, corresponding to Sr=90%), as indicated by the M2 sensor reading, water gushed out near the toe of the slope, triggering failure which propagated upward. Fig. 20 shows the cracks and small-scale failure on the slope.

4.2.3 Saturated Zone Distributions

Distributions of the saturated region and moisture content at the time of failure for Cases 8 and 9 are shown in Fig. 21. As in the earlier cases, the shaded portions correspond to fully saturated regions within the model ground as calculated from the pore water

Fig. 20 Photo showing cracks formed near the toe of the slope

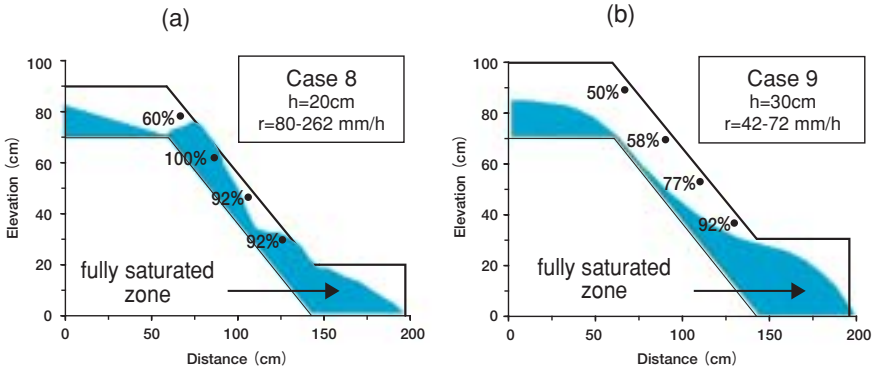

Fig. 21 Distributions of saturated zone at the time of failure: (a) Case 8; (b) Case 9 (rainfall tests)

pressure readings, whereas the numbers (in percent) are the degrees of saturation as registered by the moisture sensors whose locations are shown by black dots. In Case 8, the rainfall intensity was very high (r=262 mm/h), therefore the infiltration rate was very fast and a water table was able to form along the sloping boundary of the impervious base, inducing higher moisture contents in the surficial soil. Moreover, the 20cm thickness of the model slope allowed easy saturation of the ground. In contrast, the rainfall intensity in Case 9 was much lower (r=72 mm/h), and the thickness of the deposit was greater (h=30cm). As a result, rainwater did not accumulate along the slope. Instead it flowed downward. Consequently, only the lower portion of the slope was near full saturation at the onset of failure.

4.3 Results for Cases 1-5

As stated earlier, results for Cases 1-3 were reported elsewhere by Orense et al. (2002). In all those tests, the model slopes were made to fail by seepage of water from the water supply chamber. Consistent with the similar cases discussed above, slope failures were initiated by the formation of tension cracks on the lower part of the slope. Thereafter failure propagated to the other parts of the slope. In general, the failure surfaces formed were the non-circular retrogressive type. Slope movements within the model grounds terminated several seconds after the onset of failure. Moreover, ground deformation started only when there was full saturation of the upstream portion of the slope, indicative that full saturation not only at the toe of the slope, but of a certain region or zone upslope, precedes failure.

Comparison of the results for Cases 1 and 2, which respectively correspond to slightly steep (α=40°) and mild slopes (α=30°), showed that, assuming all factors were equal, the ground with a gentler slope failed first and more rapidly. This probably was due to the fact that as the ground water table rose during infiltration, the wetting front became parallel to the inclination of the mild slope (Case 2), and most of the ground adjacent to the surface of the slope became saturated. This is similar to what happened in Case 7. In contrast, some parts of the slightly steep slope (Case 1) were not fully saturated. As a result, slope failure occurred at a later time. Note that a more detailed seepage analysis by means of finite element method may be needed to verify this.

In Case 3, in which the model slope was similar to that in Case 1 but with a denser ground condition (Dr=70%), failure occurred at a much later time compared to Case 1 with loose ground (Dr=50%). This delayed collapse is attributed to the higher shear strength and smaller magnitude of the coefficient of permeability associated with dense ground.

An examination of the displacement of surface pins recorded by the video camera was made to investigate in detail the slope movement in Case 2. Prior to rapid displacement of the surficial portion of the slope, a minor movement was registered. At that time, saturation ratios detected by the moisture sensors were very high (nearly 100%). Movement increased for about 300 sec, reaching a magnitude of 1cm, after which rapid collapse followed.

In Cases 4-5 however, the model slopes were made to fail by the seepage of water from artificially-induced rainfall. In Case 4, a water table was not allowed to develop by draining water out of small openings in the upslope section so that a water level of 18cm was maintained in the water supply chamber. Consequently, no large-scale slope failure occurred. Instead, toe erosion caused by the water accumulated near the toe of the slope resulted in small-scale failure. Note that although failure already had started at the toe, the weak zone did not propagate to other regions. This is because the regions within the potential failure surface were not saturated enough and still had strength to resist the weight of the slope as well as the seepage forces that had developed. In Case 5, the small openings in the wall were closed and the water level was allowed to rise during rainwater infiltration. This resulted in expansion of the saturated region, and the failure that occurred near the toe immediately propagated upward as far as the mid-height of the slope.

These tests show that slope failure is not induced solely by continuous rainwater infiltration. For slope instability to occur, the water table must rise during infiltration and pore water pressure must develop. Moreover, when the water table is near the slope surface, a highly unstable zone develops, most of the time near the toe, and slope failure may be initiated in that region.

In all the tests performed, slope failures almost always occurred when soil moisture contents at specific locations approached saturated values (θs=0.42-0.43, corresponding to Sr=90-91%) This is similar to observations in Cases 6-9, evidence of the importance of monitoring changes in soil moisture contents within a slope as a possible mitigation measure.

5. DISCUSSION

5.1 Mechanism of Failure Initiation

In the series of tests discussed, two processes of rainwater infiltration for the initiation of slope failure were investigated: seepage of water from the water supply chamber upslope and seepage of water from direct rainfall. In both, failure was induced by the development of pore-water pressure due to the rise in the water level. Stress measurements were not performed in these tests, but we conjecture that the saturation process significantly reduced the effective stress and, consequently, the shear strength of the soil, specifically near the toe of the slope. This stress change caused by the hydrologic response initiated the instability of the sandy slope.

The tests also showed that continuous rainwater infiltration alone does not cause slope failure. Slope instability occurs only when the water table is allowed to rise during infiltration, and pore-water pressure develops. Moreover, when the water table approaches the slope surface, especially near the toe, a highly unstable zone is developed in that area and slope failure may be induced. This underscores the necessity of having drainage, such as gravel drains at the slope toe, to mitigate premature sliding due to locally high seepage pressure.

Once failure was initiated at the slope toe in the seepage tests, the unstable zone propagated to other portion of the slope. When the other region within the slope also has a relatively high degree of saturation (as in Case 7), it is presumed that slope failure is easily induced because of degraded strength of the adjacent ground and that retrogressive failure can occur. In contrast, the experiments using direct rainfall showed that although failure already was initiated at the toe, it did not propagate rapidly to other regions (Case 8). This is because the regions within the potential failure surface were not sufficiently saturated and still had enough strength to resist the added weight of the slope as well as the seep-

age forces that had developed.

5.2 Impending Slope Failure Warnings

Our test results revealed that there are probable indicative signs which signify the onset of slope failure during rainfall. All the tests showed that slope failures almost always are initiated when the soil moisture content in a critical region approaches a certain threshold value; in the case of Omigawa sand about θs=0.42-0.43 (corresponding to Sr=90-91%). These findings complement the results of the laboratory triaxial tests performed by Farooq et al. (2003), in which initially unsaturated soil specimens were subjected to water infiltration under a constant shear stress drained condition. Their triaxial test results showed that the soil specimen deformed slowly (small change in axial strain) during the initial phase of water infiltration. When a critical degree of saturation was reached, failure was initiated, and a rapid increase in axial strain followed. The threshold degree of saturation apparently depends on the type of soil. The degree of saturation critical for failure to occur in silty sand (fines content Fc=44%) is 93-95%, whereas for gravelly soil the threshold is lower, Sr=75-78%.

In the rainfall tests, the rise in soil moisture content was characterized by a two-step process. The first was caused by infiltration of rainwater from the slope surface toward the location of the sensor. This did not fully saturate the soil. In fact, the moisture content had a more or less constant value as the wetting front propagated toward the bottom of the slope. When it reached the impermeable base, a groundwater table was formed, and rising groundwater induced the second rise in the moisture content, ultimately leading to failure. Detecting when the second increase in moisture content would occur therefore provides a reasonable basis for predicting when a slope failure would take place.

Moreover, the rainfall tests in Cases 8 and 9 showed that cracks are formed in the upper part of the slope before large-scale deformation occurs. Such tensile cracks formed because of an increase in the weight of the surface soil and a decrease in strength at the slip surface due to increased pore water pressure. This is further magnified by the seepage forces produced by the flow of water near the interface of the impermeable base.

Minute slope deformation, commonly referred to as creep, also can serve as indicator of impending failure. A number of studies on landslides have shown that creep movement in natural slopes may be the preparatory stage for large-scale rapid slope failure (Terzaghi, 1950; Varnes, 1983; Voight, 1989; Fukuzono, 1990). Indeed, creep in slopes can provide adequate warning before there is catastrophic slope failure. For example, Punongbayan et al. (2000) reported that several months before the August 1999 landslide which buried several houses located on sloping terrain in Antipolo City, Philippines, cracks formed on the walls of some houses in the area. Some residents claimed that whenever it rained hard, there was sudden cracking of walls and windows. Other telltale signs of the impending slide (such as progressive cracking of the walls, breaking of windows and bulging of floor pavement) intensified during the height of the intense rain that began falling four days before the disastrous landslide. Taking into account the nature of creep as a precursor to landslides, creep monitoring by crack gages, extensometers, inclinometers and GPS-based systems, has commonly been adopted in conjunction with field investigations of slope instabilities, as with those that threaten cultural and historical sites (e.g., Furuya et al., 1997; Sassa et al., 2000; and Vlcko, 2004).

In our experimental tests, small-scale movement was registered prior to rapid displacement of the surficial portion of a slope by observing the motion of surface markers with digital video cameras. The same phenomenon can be observed, although less distinctly, in deformation time histories near the toe of a slope (Figs. 10(a), 12(a), 16(a) and 19(a)). When minute deformation began, volumetric moisture contents detected by moisture sensors located in critical sections of the slope ranged from θs=0.42-0.43 (Sr=90-91%). As water continued to infiltrate the soil profile, this slow, minor movement was transformed into a more rapid type of failure.

To expound on this, the results for Case 7 are presented, in which the motion of a target installed on the slope surface was observed with a laser displacement transducer. The target's location is shown by the arrow in Fig. 12, and the laser displacement transducer is positioned upslope of the target (Fig. 6b). Surface displacement readings obtained by the laser sensor (Fig. 12(b)) are converted to the equivalent shear strain by considering a 2cm thick surface soil undergoing uniform straining. The calculated shear strain time history as well as the soil moisture contents are presented in detail in Fig. 22. The figure shows that when the volumetric water content in the upper portions of the slope (M4 and M3) located far enough from the target began to increase (t=600 sec), minor deformation started at the bottom of the slope. Such movement may be associated with downward seepage forces as the wetting front moves from the top to bottom portion of the slope. Slope deformation continued to increase as water continued to seep in. When the soil moisture content in M1 location reached the threshold value (t=1300 sec), failure was triggered.

Two possible indicators of impending failure are evident from the test results presented here: (a) when the region, judged to be critical in terms of instability, becomes saturated; and (b) the detection of cracks or small magnitude of movement. By properly selecting the region in which moisture contents and displacements should be monitored, such as in areas where seepage forces may

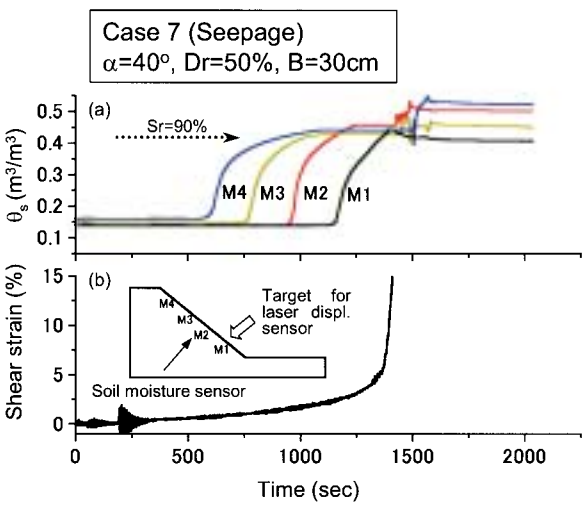

Fig. 22 Time histories of: (a) volumetric water content, θs; (b) shear strain near the toe calculated from laser displacement sensor readings in Case 7

develop, it is possible to predict when slope failures will occur. This involves knowing the temporal rate of the increase in soil moisture contents in the critical region within the slope and the threshold saturation ratios at which failure is initiated. In addition to pore water pressures, careful monitoring of soil moisture contents and slope displacement during rainwater infiltration can provide a basis for designing appropriate warning and alarm systems of slope failures caused by rainfall.

It is note-worthy that new techniques were used in the tests to measure volumetric soil moisture contents and slope deformation. The ADR-type soil moisture sensor was found to be very reliable and to provide accurate, stable soil moisture measurements on a continuous basis when properly calibrated with respect to the target soil. The shear displacement transducer, composed of vertically-arranged panels with accelerometers attached, measures not only surface displacements but sub-soil deformations as well. The readings obtained with this transducer correlate well with the movements of neighboring pin markers as recorded by video cameras. The highly-sensitive laser displacement transducer also provides accurate measurements, especially of minute slope deformations that precede large-scale failure. Although these instruments were applied to a small-scale model ground, they can be easily adapted and installed in-situ for actual field monitoring.

As stated, the results presented here were obtained in small-scale model tests under a controlled environment. Validation through numerical analyses, such as by saturated-unsaturated seepage analysis programs, and in-situ monitoring of actual slopes during rainfall are required to develop a comprehensive warning system based on changes in soil moisture content.

6. CONCLUSIONS

A series of laboratory tests were performed on small-scale model slopes to investigate onset of failure in sandy slopes caused by rainwater infiltration. Slope failure was induced by increasing the degree of saturation within the slope through seepage from the upslope section or by direct rainfall. The major findings and conclusions obtained are as follows:

(1) Slope failure always occurred when the soil moisture content within a certain region near the toe of slope became nearly fully saturated, even if other parts of the sliding mass were still only partially saturated.

(2) The threshold value of volumetric water content required for failure to occur in Omigawa sand slope with Dr=50% was θs=0.42-0.43, corresponding to Sr=90-91%.

(3) Once failure was initiated at the toe of slope, the unstable zone propagated upward to other portions of the slope. When the entire slope was under a high degree of saturation, rapid propagation of failure occurred.

(4) The failure process involved only the superficial portion of the slope with non-circular retrogressive failure surfaces.

(5) Slopes consisting of dense deposits failed later than those consisting of loose deposits because of their higher strength and lower permeability. The relative density or void ratio therefore can be used to pinpoint critical areas that may have high potential for failure.

(6) Water infiltration alone was not sufficient to induce instability. Rather, generation of pore-water pressure and increase in saturation ratios associated with the rise in the water level were necessary to create highly unstable zones.

(7) In tests in which slopes failed due to seepage of water from upslope, generally the monitored soil moisture contents showed continuous increase during infiltration until saturation was reached. In contrast, in slopes subjected to artificial rainfall, there was a two-step process; an increase associated with infiltration of water from the surface toward the location of the sensor, then a second increase caused by the rise in the groundwater table from the impermeable base.

(8) Minor slope displacements were recorded prior to rapid failure. In some cases, these were accompanied by formation of cracks upslope.

(9) New techniques to measure volumetric soil moisture contents and sub-surface soil deformations were introduced in the model tests. Although applied to small-scale ground, they are easily adapted for actual field monitoring.

(10) Two possible indicators of impending failure were evident from the experimental results: saturation of critical regions within the slope and the formation of cracks or small magnitudes of movement.

(11) The experiments showed that prediction of slope failure initiation is possible by monitoring changes in soil moisture contents and displacements within the slope, in addition to monitoring pore-water pressure. Further studies based on numerical analyses and in-situ monitoring are recommended to verify this conclusion.

ACKNOWLEDGEMENTS

This research was conducted under the auspices of Disaster Mitigation Engineering for Transport Infrastructures (Endowed Chair) sponsored by the East Japan Railway (JR-East) Company. The model tests were performed with the assistance of Messrs. T. Honda and K. Farooq of the University of Tokyo. Sampling at the Omigawa landslide site was done with the assistance of Mr. K. Ono of Civil Works Office, Chiba Prefecture and Dr. Y. Tsukamoto of Tokyo University of Science. We are deeply grateful to JR-East and the above-mentioned individuals.

REFERENCES

Brand, E. W., J. Premchitt and H. B. Phillipson, 1984. Relationship between rainfall and landslides in Hong Kong. *Proceedings, 4th International Symposium on Landslides*, Toronto, 377-384.

Chiba Prefecture Civil and River Division, 1972. *Report of Disaster in Chiba due to Autumn Rain Front of September 6-7, 1971 and Typhoon No. 25* (in Japanese).

Farooq, K., R. Orense and I. Towhata, 2003. Response of unsaturated sandy soils under constant shear stress drained condition, *Soils and Foundations*, 44 (2), 1-13.

Fukuoka, M., 1980. Landslides associated with rainfall, *Geotechnical Engineering*, 11, 1-29.

Fukuzono, T., 1990. Recent studies on time prediction of slope failure, *Landslide News*, 4, 9-12.

Furuya, G., K. Sassa, H. Fukuoka, H. Hiura, J. Wang and Q. J. Yang, 2000. Monitoring of slope deformation in Lishan Landslide, Xi'an, China, *Proceedings, 8th International Symposium on Landslides*, Cardiff,

591-596.

Kefeer, D. K., R. C. Wilson, R. K. Mark, E. E. Brabb, W, M. Brown III, S. D. Ellen, E. L. Harp, G. F. Wieczorek, C. S. Alger and R. S. Zatkin, 1987. Real-time landslide warning during heavy rainfall, *Science*, 238, 921-925.

Kitamura, R., K. Jomoto, K. Yamamoto, T. Terachi, H. Abe and T. Iryo, 1999. Field measurement of suction in soil and rainfall in Kagoshima Prefecture, *Proceedings, 1st International Symposium on Slope Stability Engineering*, Shikoku, 1, 141-145.

Kousteni, A., R. Hill, N. Dixon and J. Kavanagh, 1999. Acoustic emission technique for monitoring soil and rock slope instability, *Proceedings, 1st International Symposium on Slope Stability Engineering*, Shikoku, 1, 151-156.

Muñoz-Carpena, R., 2004. Field devices for monitoring soil water content, *Extension Bulletin 343*, Dept. of Agricultural and Biological Engineering, University of Florida.

Okada, K. and T. Sugiyama, 2001. Prediction of slope failure by critical rainfall in railway and its application, *Tsuchi-to-Kiso*, 49 (7), 22-24 (in Japanese).

Orense, R., S. Shimoma, K. Maeda, K. Farooq and I. Towhata, 2002. Laboratory model tests on rainfall-induced landslides, *Proceedings, International Symposium on Landslide Risk Mitigation and Protection of Cultural and Natural Heritage*, Kyoto, Japan, 61-71.

Punongbayan, R. S, R. A. Arboleda, R. V. Bornas and M. T. Abigania, 2000. The 3 August 1999 Landslide in Antipolo City, Philippines, *Landslide News*, 13, 12-15.

Sasahara, K., 2001. Mechanical model for prediction of steep sandy slope failure due to rainfall using surface displacement, *Tsuchi-to-Kiso*, 49 (7), 13-15 (in Japanese).

Sasaki, Y., K. Tokida, H. Matsumoto, S. Saya and T. Mori, 1991. Deformation characteristics of eccentrically loaded ground induced by soil liquefaction, *Technical Memorandum No. 3000*, Public Works Research Institute, Tsukuba, Japan.

Sassa, K., H. Fukuoka, T. Kamai and H. Shuzui, 2000. Landslide risk at Inca's World Heritage in Machu Picchu, Peru, *Landslide Risk Mitigation and Protection of Cultural and Natural Heritage*, International Geological Correlation Programme, 1, 1-14.

Shimoma, S., R. Orense, T. Honda, K. Maeda and I. Towhata, 2002. Model tests on slope failures caused by heavy rainfall, *Proceedings, Interpraevent2002 in the Pacific Rim International Congress*, Nagano, Japan, 2, 547-557.

Terzaghi, K., 1950. Mechanism of landslides, *Application of Geology to Engineering Practice*, Berkey Volume, Geological Society of America, 83-123.

Varnes, D.J., 1983. Time-deformation relations in creep to failure of earth materials, *Proceedings, 7th Southeast Asian Geotechnical Conference*, Hong Kong, 2, 107-130.

Vlcko, J., 2004. Extremely slow slope movements influencing the stability of Spis Castle, UNESCO site, *Landslides*, 1 (1), 67-71.

Voight, B., 1989. A relation to describe rate-dependent material failure, *Science*, 243, 200-203.

Wijaya, K., T. Nishimura and M. Kato, 2002. Estimation of bulk density of soil using amplitude domain reflectometry (ADR) probe, *Proceedings, 17th World Congress of Soil Science*, Bangkok, Paper No. 0385.

Wilson, R. C., J. D. Torikai and S. D. Ellen, 1992. Development of rainfall warning threshold for debris flows in Honolulu District, Oahu, *U. S. Geological Survey Open-file Report 92-521*, Washington, D.C.

Yagi, N. and R. Yatabe, 1987. Prediction method of slope failure in sandy soil due to rainfall, *Proceedings, 8th Asian Regional Conference on Soil Mechanics and Foundation Engineering*, Kyoto, 217-220.

Yokota, S., A. Iwamatsu, R. Imura, K. Matsuyuki and T. Ohkawa, 2000. A new warning index for debris flows based on rainfall and groundwater depth, *Proceedings, GeoEng2000: An International Conference on Geotechnical and Geological Engineering*, Melbourne, Paper No. SNES0481.

Yoshida, Y., J. Kuwano and R. Kuwano, 1991a. Effects of saturation on shear strength of soils, *Soils and Foundations*, 31 (1), 181-189.

Yoshida, Y., J. Kuwano and R. Kuwano, 1991b. Rain-induced slope failures caused by reduction in soil strength, *Soils and Foundations*, 31 (4), 187-193.